J. Fluid Mech. (2014), *vol.* 748, R3, doi:10.1017/jfm.2014.242

JFM RAPIDS
journals.cambridge.org/rapids

Turbulence decay towards the linearly stable regime of Taylor–Couette flow

Rodolfo Ostilla-Mónico[1,†], Roberto Verzicco[2,1], Siegfried Grossmann[3] and Detlef Lohse[1]

[1]Physics of Fluids, Mesa+ Institute, University of Twente, PO Box 217, 7500 AE Enschede, The Netherlands

[2]Dipartimento di Ingegneria Meccanica, University of Rome 'Tor Vergata', Via del Politecnico 1, Roma 00133, Italy

[3]Department of Physics, University of Marburg, Renthof 6, D-35032 Marburg, Germany

(Received 17 February 2014; revised 27 March 2014; accepted 26 April 2014)

Taylor–Couette (TC) flow is used to probe the hydrodynamical (HD) stability of astrophysical accretion disks. Experimental data on the subcritical stability of TC flow are in conflict about the existence of turbulence (cf. Ji *et al.* (*Nature*, vol. 444, 2006, pp. 343–346) and Paoletti *et al.* (*Astron. Astroph.*, vol. 547, 2012, A64)), with discrepancies attributed to end-plate effects. In this paper we numerically simulate TC flow with axially periodic boundary conditions to explore the existence of subcritical transitions to turbulence when no end plates are present. We start the simulations with a fully turbulent state in the unstable regime and enter the linearly stable regime by suddenly starting a (stabilizing) outer cylinder rotation. The shear Reynolds number of the turbulent initial state is up to $Re_s \lesssim 10^5$ and the radius ratio is $\eta = 0.714$. The stabilization causes the system to behave as a damped oscillator and, correspondingly, the turbulence decays. The evolution of the torque and turbulent kinetic energy is analysed and the periodicity and damping of the oscillations are quantified and explained as a function of shear Reynolds number. Though the initially turbulent flow state decays, surprisingly, the system is found to absorb energy during this decay.

Key words: nonlinear instability, rotating turbulence, turbulent convection

1. Introduction

Quasars are the most luminous objects in the Universe. They are thought to consist of supermassive black holes in the centres of galaxies, which accrete matter and emit radiation, thereby transforming mass into energy with an efficiency between 5 and 40 % (Ji & Balbus 2013). In order for orbiting material to move radially inwards into

† Email address for correspondence: r.ostillamonico@utwente.nl

the central object in the so-called accretion disk, it must lose its angular momentum. Molecular viscosity alone is not enough to account for this loss, so some sort of turbulent viscosity, causing the enhanced transport of angular momentum, has been conjectured (Shakura & Sunyaev 1973), as otherwise gravitationally bound objects, such as quasars, stars or planets, would not exist. This implies that the flow of the material must be turbulent, but the origin of turbulence in some types of accretion disks is currently disputed. Accretion disks can either be 'hot', and therefore highly ionized and electrically conducting, or 'cold', and therefore extremely poorly ionized and poorly electrically conducting. Hot disks are found around quasars and active galactic nuclei, and thought to undergo a magneto-rotational instability (MRI) to become turbulent (Velikhov 1959; Balbus & Hawley 1991). In contrast, cold disks are found in protoplanetary systems, and are thought to have 'MRI-dead' regions where turbulence due the MRI cannot exist as the magnetic Reynolds number is too low (Gammie 1996; Armitage 2011). The places where planets eventually form and reside coincide with these MRI-dead regions, so additional transport of angular momentum must take place. To account for this transport another mechanism to generate turbulence has been proposed: hydrodynamical (HD) nonlinear instabilities.

Taylor–Couette (TC) flow is the flow between two coaxial cylinders which rotate independently. It is used as a model for probing the HD stability of accretion disks (Ji & Balbus 2013). Accretion disks have velocity profiles that are linearly stable, but, just as in pipe and channel flows, the shear Reynolds numbers are so large that nonlinear instabilities may play a role in the formation of turbulence. The question whether TC flow does indeed undergo a nonlinear transition (Trefethen *et al.* 1993; Grossmann 2000) to turbulence at large shear Reynolds numbers has been probed experimentally by several authors, with conflicting results (Richard 2001; Dubrulle *et al.* 2005; Ji *et al.* 2006; Paoletti & Lathrop 2011; van Gils *et al.* 2011, 2012; Avila 2012; Paoletti *et al.* 2012; Schartman *et al.* 2012). The discrepancies between the different experiments have been attributed to the end plates of the TC devices, i.e. the solid boundaries which axially confine TC flow. These cause secondary flows, known as Ekman circulation, which propagate into the flow and influence global stability. Avila (2012), based on his numerical simulations with end plates imitating the Ji *et al.* (2006) and Paoletti *et al.* (2012) experiments, concluded that both of these experiments were inadequate to study the nonlinear transition due to the presence of end plates. However, these simulations are at shear Reynolds numbers of the order of $Re_s \sim 10^4$, while Ji *et al.* (2006) mention the counter-intuitive result that Re_s must exceed a certain threshold before the flow relaminarizes.

Indeed, confinement of the flow plays a very important role in this transition, but it is unavoidable in experiments. Direct numerical simulations (DNS) do not have these limitations, as they can be run with periodic boundary conditions to completely prevent end-plate effects. Following this idea, Lesur & Longaretti (2005) simulated rotating plane Couette flow with perturbed initial conditions, going up to shear Reynolds numbers of the order of 10^4; however, due to computational limitations, the quasi-Keplerian regime velocity (i.e. the regime where the two velocity boundary conditions are related by Kepler's third law) was not reached.

In this manuscript, we adopt a similar approach, but now for TC flow and, in particular, reaching larger shear Reynolds numbers $Re_s \sim 10^5$. We proceed as follows: we start from a turbulent flow field, corresponding to a pure inner cylinder rotation in the laboratory frame, and then switch on stabilizing outer cylinder rotation, wondering whether the turbulence is sustained. We find that it is not: the turbulence decays, and the torque decreases down to a value corresponding to purely azimuthal, laminar flow. This means that not only the TC system is linearly stable in this geometry, but even an initially turbulent flow decays towards the linearly stable regime.

2. Numerical details

The DNS were performed using a second-order finite difference code with fractional time-stepping (Verzicco & Orlandi 1996). This code has already been validated and used extensively in the context of TC flow (Ostilla *et al.* 2013; Ostilla-Monico *et al.* 2014). The turbulent initial conditions are taken from Ostilla-Monico *et al.* (2014). The radius ratio is $\eta = r_i/r_o = 0.714$, where r_i and r_o are the inner and outer radii, respectively, and the spatial period aspect ratio is $\Gamma = L/d = 2.094$, where L is the axial periodicity length and d the gap width $d = r_o - r_i$. A rotational symmetry of order six was forced on the system to reduce computational costs while not affecting the results (Brauckmann & Eckhardt 2013; Ostilla-Monico *et al.* 2014). With this rotational symmetry, the system has an azimuthal periodic length of $L_\theta/d = 3.141$ at the mid-gap.

The simulations are performed in a frame of reference co-rotating with the outer cylinder. In the rotating frame, the inner cylinder has an azimuthal velocity $U = r_i(\omega_i - \omega_o)$, with ω_i and ω_o the inner and outer cylinder angular velocities, respectively, while the outer cylinder is now stationary. The resulting shear drives the flow and can be expressed non-dimensionally as a shear Reynolds number (we note that in the astrophysical context, e.g. Dubrulle *et al.* (2005), often an extra factor $2/(1+\eta)$ is used in this definition) $Re_s = dU/\nu$, where ν is the kinematic viscosity of the fluid. In this rotating frame, the outer cylinder rotation in the lab frame manifests itself as a Coriolis force $Ro^{-1}(\boldsymbol{e}_z \times \boldsymbol{u})$, where the Rossby number is defined as $Ro = U/(2\omega_o d) = (\eta[1-\mu])/(2\mu[1-\eta])$, with $\boldsymbol{e}_z$ the unit vector in the axial direction and $\mu = \omega_o/\omega_i$ the angular velocity ratio (in the stationary lab system). Note that Ro can be either negative or positive. We define the non-dimensional radius as $\tilde{r} = (r - r_i)/d$, the non-dimensional axial height as $\tilde{z} = z/d$ and the non-dimensional time as $\tilde{t} = tU/d$, where d/U is the large-eddy turnover time of the initial state.

Six simulations were run: three with fixed $Re_s = 8.10 \times 10^3$, but different strengths of the Coriolis force, namely: (*a*) $Ro^{-1} = 0.83$, corresponding to a system on the Rayleigh stability line, equivalent to $r_i^2\omega_i = r_o^2\omega_o$, or $\mu = \eta^2 \approx 0.51$ in the lab frame of reference; (*b*) $Ro^{-1} = 1.22$, corresponding to $\mu = \eta^{3/2} \approx 0.60$ or a system in the quasi-Keplerian regime, i.e. the regime in which the angular velocities at the two cylinders are related by Kepler's third law $r_i^3\omega_o^2 = r_o^3\omega_i^2$; and (*c*) $Ro^{-1} = 2.50$, an even stronger stabilization, equivalent to $\mu \approx 0.76$. The other three simulations were done by fixing $Ro^{-1} = 1.22$ and using the values $Re_s = 8.10 \times 10^3$, $Re_s = 2.52 \times 10^4$ and $Re_s = 8.10 \times 10^4$. Grids of $N_\theta \times N_r \times N_z = 256 \times 640 \times 512$ were used for all simulations, except for $Re_s = 8.10 \times 10^4$, where a grid of $N_\theta \times N_r \times N_z = 512 \times 800 \times 1024$ is required to guarantee sufficient resolution. The adequacy of these meshes for the simulated Re_s was demonstrated in Ostilla-Monico *et al.* (2014). Figure 1 shows an overview of how the initial conditions from the Rayleigh-unstable regime were moved across the phase space by adding the Coriolis force.

Simulating in a rotating frame adds a new perspective to the problem. In this frame the (non-dimensional) Navier–Stokes equations read:

$$\frac{\partial \hat{\boldsymbol{u}}}{\partial \hat{t}} + \hat{\boldsymbol{u}} \cdot \hat{\nabla}\hat{\boldsymbol{u}} = -\hat{\nabla}\hat{p} + \frac{1}{Re_s}\hat{\nabla}^2\hat{\boldsymbol{u}} - Ro^{-1}\boldsymbol{e}_z \times \hat{\boldsymbol{u}}, \tag{2.1}$$

where $\hat{\boldsymbol{u}}$ is the non-dimensional velocity and $\hat{t}$ the non-dimensional time. Strong enough outer cylinder co-rotation in the lab-frame implies a large stabilizing Coriolis force Ro^{-1} in the rotating frame, leading to suppression of the turbulence as the

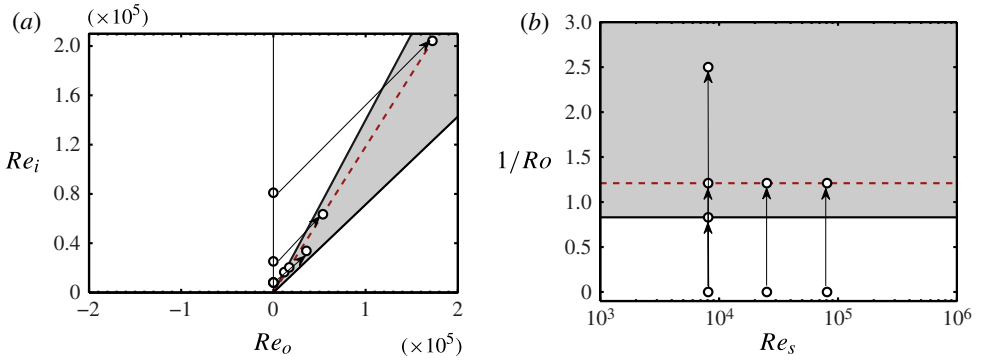

FIGURE 1. Initial conditions and simulations run in the (Re_i, Re_o) phase space (a) and the $(Re_s, 1/Ro)$ phase space (b). The shaded region indicates the zone for which angular velocity is transported outwards $\omega_o \leqslant \omega_i$, and angular momentum is transported inwards $r_i^2\omega_i \leqslant r_o^2\omega_o$, i.e. the flow is Rayleigh stable and can be formulated in the rotating frame as $\omega_i > \omega_o$. The dashed line indicates quasi-Keplerian boundary conditions. The arrows indicate the movement of the initial conditions from pure inner cylinder rotation to the Rayleigh-stable states by adding a Coriolis force.

large-scale balance in the bulk between the angular velocity gradient and the Coriolis force is broken (Ostilla *et al.* 2013). This argument for stabilization can be compared to that of Taylor–Proudman's theorem (Proudman 1916; Taylor 1917), which when applied to rotating Rayleigh–Bénard flow implies that the flow is stable even at large thermal driving, as long as the background rotation is large enough (Chandrasekhar 1981).

3. Results and analysis

Figure 2 shows three instantaneous snapshots of the angular velocity ω for $Re_s = 8.10 \times 10^3$ at times $\tilde{t} = 0$, $\tilde{t} = 3.1$ and $\tilde{t} = 6.2$ after the stabilizing Coriolis force corresponding to the quasi-Keplerian regime, $Ro^{-1} = 1.22$, was added. The sequence of figures shows the reversal of the Taylor vortices, which occurs with a period of $\tilde{t} \approx 6.2$. If the system is simulated for a large enough time, here $\tilde{t} \sim 200$, the Taylor vortices progressively fade away. The system behaves approximately as a damped oscillator.

To quantify these reversals, we define the quasi-Nusselt number (Eckhardt, Grossmann & Lohse 2007) $Nu_\omega(r, t)$ as $Nu_\omega(r, t) = r^3(\langle u_r\omega\rangle_{\theta,z} - \nu\partial_r\langle\omega\rangle_{\theta,z})/T_{pa}$, where T_{pa} is the torque required to drive the system in the purely azimuthal and laminar case, r is the radius, u_r is the radial velocity, ω the angular velocity and $\langle\ldots\rangle_\phi$ indicates averaging with respect to variable ϕ. Here $Nu_\omega(r, t)$ represents the transport of angular velocity. For a purely azimuthal flow with no turbulence, $Nu_\omega = 1$, and therefore $Nu_\omega - 1$ represents the additional transport of angular velocity due to turbulence.

Figure 3 shows a time series of the axially averaged $Nu_\omega - 1$ at the mid-radius $\tilde{r} = 0.5$, for $Re_s = 8.10 \times 10^3$ and $Ro^{-1} = 1.22$. Here, $Nu_\omega - 1$ can be seen to oscillate between large positive and large negative values, with an average of approximately zero, i.e. no net turbulent transport. For large enough times ($\tilde{t} > 3000$), the oscillations damp out and the flow becomes purely azimuthal and laminar, $Nu_\omega = 1$. In the other simulations, the period of oscillation depends strongly on Ro^{-1} (decreasing with increasing Ro^{-1}) but only weakly on Re_s. Oscillations can be seen even if

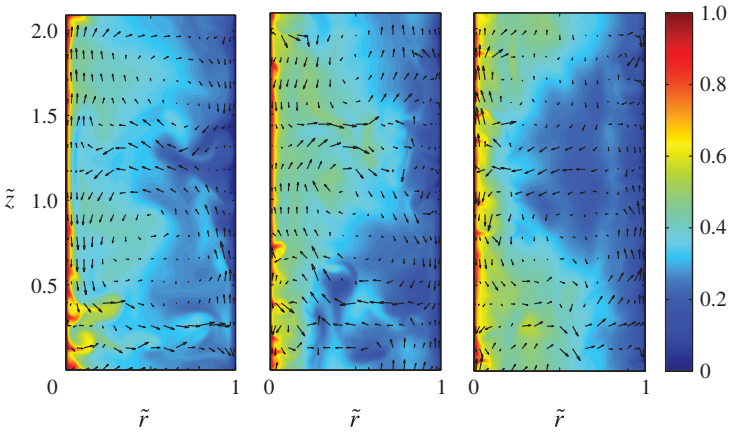

FIGURE 2. Snapshots of contour plots of the instantaneous angular velocity field ω for $Re_s = 8.10 \times 10^3$, $Ro^{-1} = 1.22$. Arrows represent the underlying axial and radial velocities. The snapshot on the left shows the initial field at $\tilde{t} = 0$, while in the two later snapshots (at $\tilde{t} = 3.1$ and $\tilde{t} = 6.2$) reversals of the Taylor rolls can be seen: the radial velocity in the gap at mid-height ($\tilde{z} \approx 1.1$) changes from inwards in the first snapshot, to outwards in the second, and back again to inwards in the last. See supplementary movie available at http://dx.doi.org/10.1017/jfm.2014.242.

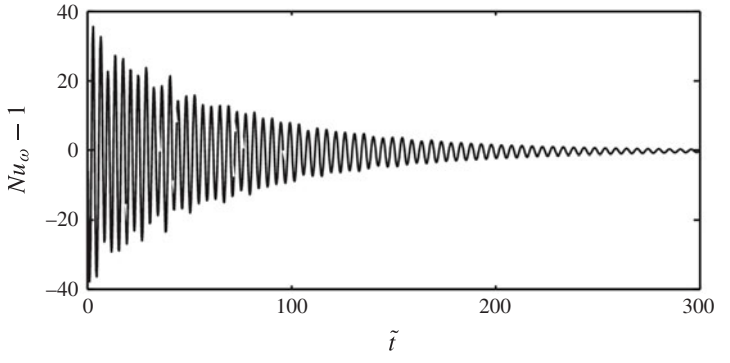

FIGURE 3. Time series of $Nu_\omega - 1$ at mid-gap for $Re_s = 8.10 \times 10^3$ and $Ro^{-1} = 1.22$, (quasi-Keplerian). Large oscillations of $Nu_\omega - 1$ from positive to negative can be seen, which, when averaged, show that there is no net turbulent transport of angular velocity. The fluctuations decay with time. For a long enough time $\tilde{t} \approx 3000$, they stop and $Nu_\omega - 1$ finally stabilizes at zero.

a non-stabilizing co-rotation is added, but the system does not return to a purely azimuthal state with $Nu_\omega = 1$. Instead, after some oscillations in which Nu_ω decreases, a new turbulent state with $Nu_\omega > 1$ is reached.

Figure 4 shows the axially averaged $Nu_\omega - 1$, but now measured directly at the inner cylinder (probing the inner boundary layer (BL)) for different values of Ro^{-1} and Re_s. Unlike the previous mid-gap case, no oscillations can be seen, reflecting that the oscillations occur only in the bulk of the flow, where the Taylor vortices are, but that

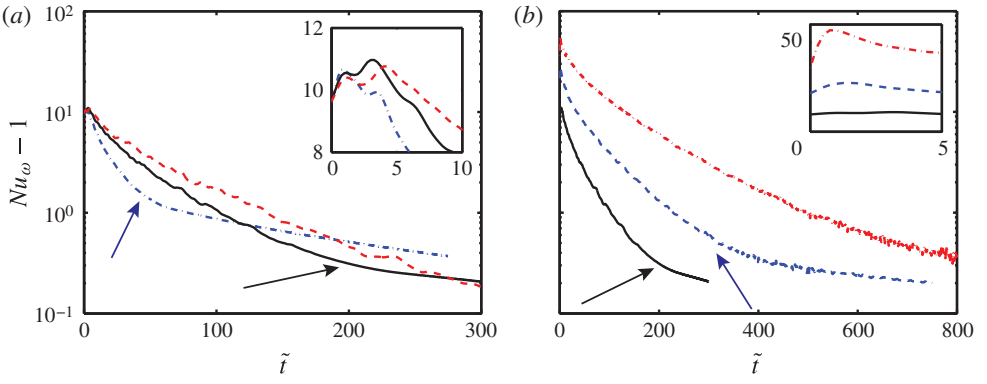

FIGURE 4. (*a*) Semi-log time series of $Nu_\omega - 1$ at the inner cylinder ($\tilde{r} = 0$, z-averaged) for $Re_s = 8.10 \times 10^3$ and three values of Ro^{-1}. Red dashed line, $Ro^{-1} = 0.83$ (Rayleigh stability line); black line, $Ro^{-1} = 1.22$ (quasi-Keplerian); blue dash-dot line, $Ro^{-1} = 2.50$. (*b*) Semi-log time series of $Nu_\omega - 1$ at the inner cylinder for $Ro^{-1} = 1.22$ and three values of Re_s (black line, $Re_s = 8.10 \times 10^3$; blue dashed line, $Re_s = 2.52 \times 10^4$; red dash-dot line, $Re_s = 8.10 \times 10^4$). Two decay modes can be seen in this figure, with the crossovers marked with arrows. In both (*a*) and (*b*), fluctuations are absent, unlike at the mid-gap, but $Nu_\omega - 1$ decays. For a large enough time, $Nu_\omega - 1$ drops to zero, taking more time to do so for higher Re_s or for smaller Ro^{-1}. Zoom-ins of the first few large-eddy turnover times are shown as insets (linear scale) for both figures. Transients, corresponding to an increase of Nu_ω, can be seen during the initial stages.

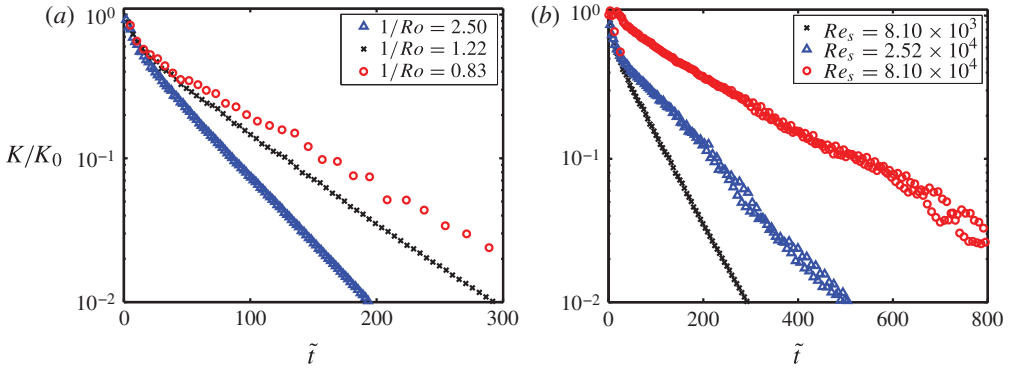

FIGURE 5. (*a*) Time series of $K(\tilde{t})/K_0$ for $Re_s = 8.10 \times 10^3$ and three values of Ro^{-1}: $Ro^{-1} = 0.83$ (Rayleigh stability line), $Ro^{-1} = 1.22$ (quasi-Keplerian) and $Ro^{-1} = 2.50$. (*b*) Time series of K/K_0 for $Ro^{-1} = 1.22$ and three values of Re_s. After the initial transient, an exponential decay of the turbulent kinetic energy can be seen, even at the largest Reynolds numbers.

the BLs are unaffected. Of course, the decay towards the purely azimuthal, laminar state $Nu_\omega = 1$ is also observed in the BLs (figure 4*a*,*b*), independent of Ro^{-1} and Re_s.

Finally, we quantify the decay of turbulence. To do so, we define the turbulent kinetic energy substitute of the flow as $K(t) = \langle u_r^2 + u_z^2 \rangle_{r,z,\theta}/2$. Note that this is not the full turbulent energy, as for that also fluctuations in u_θ contribute, but, by definition, K has the desirable property of being zero in the purely azimuthal state. Figure 5(*a*)

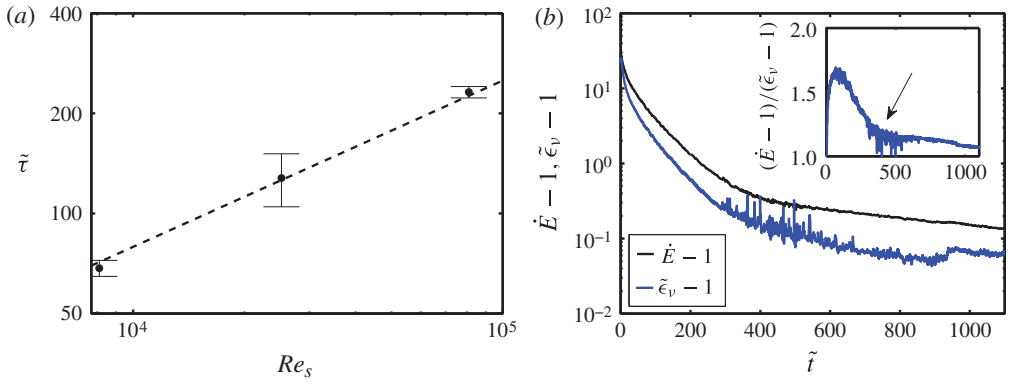

FIGURE 6. (*a*) Log–log plot of the turbulence decay time $\tilde{\tau}$ versus Re_s for $Ro^{-1} = 1.22$ (quasi-Keplerian) and the three values of Re_s simulated. The dashed line shows the power law $\tilde{\tau} = 0.79\sqrt{Re_s}$ fit to the data points. (*b*) Semi-logarithmic plot of the time series of both the energy input through the boundaries $\dot{E} - 1$ and the viscid dissipation of energy in the system $\tilde{\epsilon}_v - 1$ for $Re_s = 2.49 \times 10^4$ and $Ro^{-1} = 1.22$. The laminar dissipation – i.e. unity, with the non-dimensionalization chosen – is subtracted from both variables. The inset shows the ratio between both energies. The arrow marks the transition between the two decay mechanisms. For a considerable time, the system still absorbs more energy than it dissipates; equilibrium is reached only for $\tilde{t}$ beyond 1000, due to the small decay rate.

shows the decay of K for $Re_s = 8.10 \times 10^3$ and three values of Ro^{-1}, while figure 5(*b*) shows the decay for $Ro^{-1} = 1.22$ and three values of Re_s. In the simulations, $K(\tilde{t})$ shows fluctuations with a short time scale, similar to that of Nu_ω in the mid-gap, so for clarity only the peak of $K(\tilde{t})$ in every cycle is represented.

As expected from the previous results on $Nu_\omega(\tilde{t}) - 1$, $K(\tilde{t})$ decays to zero when given enough time. The only mechanism for energy dissipation is viscosity, so it is not surprising that the decay time is proportional to the energy content, thus leading to an approximately exponential decay, $K(\tilde{t}) = K_0 \exp(-\tilde{t}/\tilde{\tau})$, where $\tilde{\tau}$ is the characteristic (dimensionless) decay time and $K_0 = K(\tilde{t} = 0)$. Fits to the data in figure 5(*b*) were performed to obtain estimates for the dependence $\tilde{\tau}(Re_s)$, which is shown in figure 6(*a*). The absolute value of $\tilde{\tau}$ is large (around 70 large-eddy turnover times for $Re_s \sim 10^4$ and $Ro^{-1} = 1.22$) and in the range studied shows a power law

$$\tilde{\tau} \sim \sqrt{Re_s}. \tag{3.1}$$

This scaling can be understood by realizing that the decay of the turbulence is first dominated by the energy dissipation rate ϵ_{BL} in the BLs, which scales as (Grossmann & Lohse 2000) $\epsilon_{BL} \sim \nu^3 d^{-4} Re_s^{5/2}$. This immediately implies the scaling relation (3.1) for the typical decay time $\tau = \tilde{\tau} d/U \sim U^2/\epsilon_{BL}$. Only for very large times or for very small Reynolds numbers from the very beginning, i.e. when the thickness of the BLs is comparable to the gap thickness d and the Taylor rolls have died out or are absent, does $\epsilon_{BL} \sim \nu^3 d^{-4} Re_s^2$ (cf. Grossmann & Lohse (2001)) and thus $\tau \sim Re_s$. This second regime can be seen in figures 4(*b*) and 6(*b*).

We highlight that even though $K(\tilde{t})$ decays, the total energy of the system increases, as it absorbs more energy through the boundaries than it dissipates viscidly. This can be seen in figure 6(*b*), which shows a time series of the non-dimensionalized energy input into the system $\dot{E} = (T_i\omega_i + T_o\omega_o)/(\rho\Omega\epsilon_{pa})$, where $T_{i,o}$ is the torque

applied at the inner (outer) cylinder, ρ and Ω are the fluid density and volume, respectively, and ϵ_{pa} is the viscous dissipation in the purely azimuthal and laminar state, and a time series of the non-dimensionalized energy dissipationrate inside the system, $\tilde{\epsilon}_\nu = \nu\langle[\partial_i u_j + \partial_j u_i]^2\rangle_{r,\theta,z}/\epsilon_{pa}/2$. When transitioning from turbulence to the purely azimuthal $u_\theta(r)$-profile, the system absorbs energy, while at the same time the initial turbulence decays. The purely azimuthal $u_\theta(r)$-profile has more energy than its turbulent counterpart. Indeed, this is the reason for the Rayleigh instability, now supressed by the Coriolis force.

Again, two time scales for the decay can be seen in the inset of figure 6(*b*). After the initial transient, turbulence in the bulk decays rapidly, due to the efficient angular momentum transport by the Taylor rolls. After approximately 200–300 large-eddy turnover times this decay mechanism is exhausted, as then the (turbulent) Taylor rolls in the bulk are so weak that they can no longer transport angular momentum. Then a second decay mechanism takes over, whose onset is marked by an arrow in the inset of figure 6(*b*). In this regime, characterized by purely viscous dissipation $\sim \nu^3 L^{-4} Re_s^2$ in the whole gap, the profile $u_\theta(r)$ returns to the laminar form and Nu_ω thus becomes unity. It is important to note that Nu_ω must return to unity, because in the statistically stationary state Nu_ω must be independent of r.

4. Summary and conclusions

In summary, consistent with what had been found in the experiments of Ji *et al.* (2006) and Schartman *et al.* (2012), no turbulence and, therefore, no turbulent transport of angular momentum can be seen in the Rayleigh-stable regime for the control parameter range studied once the effect of axial boundaries is mitigated. An initially turbulent state is stabilized by the co-rotation of the outer cylinder and the transport of angular momentum in the bulk ceases; the turbulence decays in all our simulations, for Re_s up to 8.10×10^4.

We point out, however, that even though the system is stable, the decay times for turbulence are long, ranging between hundreds and thousands of large-eddy turnover times. If one extrapolates the scaling relation (3.1) to shear Reynolds numbers attainable in cold accretion disks, which are of the order of 10^{14}, decay times for the turbulence become very large. This is done ignoring possible crossovers to an ultimate regime in which the energy dissipation rate may be dominated by the bulk dissipation (Grossmann & Lohse 2000, 2011) $\epsilon_{bulk} \sim \nu^3 d^{-4} Re_s^3$. In that regime $\tilde{\tau}$ would become independent of Re_s. Indeed, for astrophysical disks without inner- and outer-boundary layers, we expect this to be the case. Viscous dissipation would be dominated by the bulk dynamics, and (3.1) would not be applicable.

The decay times observed in the simulations are in discrepancy with experiments by Borrero-Echeverry, Schatz & Tagg (2010) and Edlund & Ji (2014). Edlund & Ji (2014) use a similar set-up to that of Ji *et al.* (2006), but now switch on and off a pump to perturb the quiescent TC flow with quasi-Keplerian boundary conditions. The decay time of the perturbation is much smaller than those observed in the DNS. The discrepancy in time scale can probably be attributed to increased bulk dissipation at higher Re and to end-plate effects, which increase the dissipation of the system. On the other hand, Borrero-Echeverry *et al.* (2010) showed that for pure outer cylinder rotation, perturbations decay stochastically (i.e. are memoryless). The decay times grow superexponentially, and thus are much larger than those seen in the DNS. Turbulent dynamics can be seen before the relaminarization, and a mechanism by which turbulence regenerates is present. We point out that for pure outer cylinder

rotation, TC flow transports angular velocity inwards, and this completely changes the dynamics of the problem, thus causing a different behaviour in the decay.

It is also unclear whether the extreme values of η present in astrophysical accretion disks will have an effect on the decay times. The Rossby number has a strong η-dependence, and for $\eta \to 0$ it diverges. Other types of mechanism might dominate the angular momentum transport in cold accretion disks. These are axially stratified in density, and thus other types of instability, such as subcritical baroclinic instabilities (Withjack & Chen 1974; Klahr & Bodenheimer 2003; Petersen, Julien & Stewart 2007), can be present. Finally, transport associated with self-gravity (Paczynski & Bisnovatyi-Kogan 1981) may also play a role. We refer the reader to Armitage (2011) for a more detailed discussion.

In conclusion, in our TC simulations without end plates, in the parameter range studied up to shear Reynolds numbers of 10^5, the flow was seen to not only remain laminar in the presence of small perturbations, but also when starting from an initially turbulent state the turbulence decays and the system returns to its laminar state. All of this happens while the system absorbs energy. Our findings extend the results from Avila (2012), who also attributed the turbulence and increased angular momentum transport found in some of the experiments (Dubrulle *et al.* 2005; Paoletti & Lathrop 2011) which probe the linearly stable regime of TC flow to the effects of end-plate confinement.

Initial conditions are taken from the Rayleigh-unstable region, and thus are dominated by toroidal Taylor vortices with a strong axial dependence. These are chosen as they are as general as possible. When the stabilizing rotation is switched on, the Taylor–Proudman theorem impiles that these vortices cannot be sustained, and thus vanish. It is worth noting that if different boundary conditions are used, such as radial inflow (Gallet, Doering & Spiegel 2010) or differentially heated cylinders (Lopez, Marques & Avila 2013), Taylor columns which have no axial dependence may develop. However, with the basic TC boundary conditions, these structures do not develop, as the system might be too constrained. This result is in agreement with theoretical work by Rincon, Ogilvie & Cossu (2008), who reach a similar conclusion for plane Couette flow, as the nonlinear mechanisms appear to be fundamentally differently beyond the Rayleigh stability line. An analysis based on linear transient growth, such as done by Maretzke, Hof & Avila (2014), which also predicts columnar structures as the optimal initial conditions, may thus not be valid for determining the stability of TC flow at high Reynolds numbers.

Supplementary movie

A supplementary movie is available at http://dx.doi.org/10.1017/jfm.2014.242.

References

ARMITAGE, P. J. 2011 Dynamics of protoplanetary disks. *Annu. Rev. Astron. Astrophys.* **49**, 195–236.

AVILA, M. 2012 Stability and angular-momentum transport of fluid flows between corotating cylinders. *Phys. Rev. Lett.* **108** (12), 124501.

BALBUS, S. A. & HAWLEY, J. 1991 A powerful local shear instability in weakly magnetized disks. *Astrophys. J.* **376**, 214–233.

BORRERO-ECHEVERRY, D., SCHATZ, M. F. & TAGG, R. 2010 Transient turbulence in Taylor–Couette flow. *Phys. Rev.* E **81**, 025301.

BRAUCKMANN, H. & ECKHARDT, B. 2013 Direct numerical simulations of local and global torque in Taylor–Couette flow up to $Re = 30\,000$. *J. Fluid Mech.* **718**, 398–427.

CHANDRASEKHAR, S. 1981 *Hydrodynamic and Hydromagnetic Stability*. Dover.

DUBRULLE, B., DAUCHOT, O., DAVIAUD, F., LONGARETTI, P. Y., RICHARD, D. & ZAHN, J. P. 2005 Stability and turbulent transport in Taylor–Couette flow from analysis of experimental data. *Phys. Fluids* **17**, 095103.

ECKHARDT, B., GROSSMANN, S. & LOHSE, D. 2007 Torque scaling in turbulent Taylor–Couette flow between independently rotating cylinders. *J. Fluid Mech.* **581**, 221–250.

EDLUND, E. M. & JI, H. 2014 Nonlinear stability of laboratory quasi-Keplerian flows. *Phys. Rev.* E **89**, 021004.

GALLET, B., DOERING, C. R. & SPIEGEL, E. A. 2010 Destabilizing Taylor–Couette flow with suction. *Phys. Fluids* **22**, 034105.

GAMMIE, C. F. 1996 Layered accretion in T-Tauri disks. *Astrophys. J.* **457**, 355–362.

GROSSMANN, S. 2000 The onset of shear flow turbulence. *Rev. Mod. Phys.* **72**, 603–618.

GROSSMANN, S. & LOHSE, D. 2000 Scaling in thermal convection: a unifying view. *J. Fluid Mech.* **407**, 27–56.

GROSSMANN, S. & LOHSE, D. 2001 Thermal convection for large Prandtl number. *Phys. Rev. Lett.* **86**, 3316–3319.

GROSSMANN, S. & LOHSE, D. 2011 Multiple scaling in the ultimate regime of thermal convection. *Phys. Fluids* **23**, 045108.

JI, H. & BALBUS, S. A. 2013 Angular momentum transport in astrophysics and in the lab. *Phys. Today* **66** (8), 27–33.

JI, H., BURIN, M., SCHARTMAN, E. & GOODMAN, J. 2006 Hydrodynamic turbulence cannot transport angular momentum effectively in astrophysical disks. *Nature* **444**, 343–346.

KLAHR, H. H. & BODENHEIMER, P. 2003 Turbulence in accretion disks: vorticity generation and angular momentum transport via the global baroclinic instability. *Astrophys. J.* **508** (2), 869–892.

LESUR, G. & LONGARETTI, P. Y. 2005 On the relevance of subcritical hydrodynamic turbulence to accretion disk transport. *Astron. Astrophys.* **444**, 25–44.

LOPEZ, J. M., MARQUES, F. & AVILA, M. 2013 The Boussinesq approximation in rapidly rotating flows. *J. Fluid Mech.* **737**, 56–77.

MARETZKE, S., HOF, B. & AVILA, M. 2014 Transient growth in lineraly stable Taylor–Couette flows. *J. Fluid Mech.* **742**, 254–290.

OSTILLA, R., STEVENS, R. J. A. M., GROSSMANN, S., VERZICCO, R. & LOHSE, D. 2013 Optimal Taylor–Couette flow: direct numerical simulations. *J. Fluid Mech.* **719**, 14–46.

OSTILLA-MONICO, R., VAN DER POEL, E. P., VERZICCO, R., GROSSMANN, S. & LOHSE, D. 2014 Boundary layer dynamics at the transition between the classical and the ultimate regime of Taylor–Couette flow. *Phys. Fluids* **26**, 015114.

PACZYNSKI, B. & BISNOVATYI-KOGAN, G. 1981 A model of a thin accretion disk around a black hole. *Acta Astron.* **31** (3), 283–291.

PAOLETTI, M. S. & LATHROP, D. P. 2011 Angular momentum transport in turbulent flow between independently rotating cylinders. *Phys. Rev. Lett.* **106**, 024501.

PAOLETTI, M. S., VAN GILS, D. P. M., DUBRULLE, B., SUN, C., LOHSE, D. & LATHROP, D. P. 2012 Angular momentum transport and turbulence in laboratory models of Keplerian flows. *Astron. Astrophys.* **547**, A64.

PETERSEN, M. R., JULIEN, K. & STEWART, G. R. 2007 Baroclinic vorticity production in protoplanetary disks. I. Vortex formation. *Astrophys. J.* **658**, 1236–1251.

PROUDMAN, J. 1916 On the motion of solids in a liquid possessing vorticity. *Proc. R. Soc. Lond.* A **92**, 408–424.

RICHARD, D. 2001 Instabilités hydrodynamiques dans les ecoulements en rotation différentielle. PhD thesis, University of Paris 7.

RINCON, F., OGILVIE, G. I. & COSSU, C. 2008 On self-sustaining processes in Rayleigh-stable rotating plane Couette flows and subcritical transitions to turbulence in accretion disks. *Astron. Astrophys.* **463**, 817–832.

SCHARTMAN, E., JI, H., BURIN, M. J. & GOODMAN, J. 2012 Stability of quasi-Keplerian shear flow in a laboratory experiment. *Astron. Astrophys.* **543**, A94.

SHAKURA, N. I. & SUNYAEV, R. A. 1973 Black holes in binary systems. Observational appearance. *Astron. Astrophys.* **24**, 337–355.

TAYLOR, G. I. 1917 Motion of solids in fluids when the flow is not irrotational. *Proc. R. Soc. Lond.* A **93**, 92–113.

TREFETHEN, L. N., TREFETHEN, A. E., REDDY, S. C. & DRISCOL, T. A. 1993 Hydrodynamic stability without eigenvalues. *Science* **261**, 578–584.

VAN GILS, D. P. M., HUISMAN, S. G., BRUGGERT, G. W., SUN, C. & LOHSE, D. 2011 Torque scaling in turbulent Taylor–Couette flow with co- and counter-rotating cylinders. *Phys. Rev. Lett.* **106**, 024502.

VAN GILS, D. P. M., HUISMAN, S. G., GROSSMANN, S., SUN, C. & LOHSE, D. 2012 Optimal Taylor–Couette turbulence. *J. Fluid Mech.* **706**, 118–149.

VELIKHOV, E. P. 1959 Stability of an ideally conducting liquid flowing between rotating cylinders in a magnetic field. *Zh. Eksp. Teor. Fiz.* **36**.

VERZICCO, R. & ORLANDI, P. 1996 A finite-difference scheme for three-dimensional incompressible flow in cylindrical coordinates. *J. Comput. Phys.* **123**, 402–413.

WITHJACK, E. M. & CHEN, C. F. 1974 An experimental study of Couette instability of stratified fluids. *J. Fluid Mech.* **66**, 725–737.